ORIGINAL ARTICLE

Superaerophobic graphene nano-hills for direct hydrazine fuel cells

Kamran Akbar[1], Jung Hwa Kim[2], Zonghoon Lee[2], Minsoo Kim[3], Yeonjin Yi[3] and Seung-Hyun Chun[1]

Hydrazine fuel-cell technology holds great promise for clean energy, not only because of the greater energy density of hydrazine compared to hydrogen but also due to its safer handling owing to its liquid state. However, current technologies involve the use of precious metals (such as platinum) for hydrazine oxidation, which hinders the further application of hydrazine fuel-cell technologies. In addition, little attention has been devoted to the management of gas, which tends to become stuck on the surface of the electrode, producing overall poor electrode efficiencies. In this study, we utilized a nano-hill morphology of vertical graphene, which efficiently resolves the issue of the accumulation of gas bubbles on the electrode surface by providing a nano-rough-edged surface that acts as a superaerophobic electrode. The growth of the vertical graphene nano-hills was achieved and optimized by a scalable plasma-enhanced chemical vapor deposition method. The resulting metal-free graphene-based electrode showed the lowest onset potential (−0.42 V vs saturated calomel electrode) and the highest current density of all the carbon-based materials reported previously for hydrazine oxidation.
NPG Asia Materials (2017) **9**, e378; doi:10.1038/am.2017.55; published online 19 May 2017

INTRODUCTION

Among the many clean and sustainable energy-harvesting technologies, direct liquid fuel cells stand out due to several promising features: high energy and power density, greatly enhanced fuel-to-energy conversion efficiency (especially compared with combustion engines), the ability for use at remote locations (including in space), and the availability of a wide variety of liquid fuels (for example, methanol, hydrazine, ethanol and higher hydrocarbons).[1] Hydrazine as a liquid fuel for direct liquid fuel cells outshines others not only because of its high theoretical cell voltage (+1.61 V) but also due to its greater energy and power density compared with other fuels, especially hydrogen, which has traditionally been a standard due to its widespread use in various fuel-cell technologies.[2]

However, the practical energy conversion efficiencies of hydrazine-based direct liquid fuel cells are lower than their theoretical values, mostly due to the requirement of a substantial overpotential for hydrazine oxidation; hence, an electrocatalyst is normally needed. So far, platinum is considered to be the best electrocatalyst for hydrazine oxidation with the lowest onset potential, but its price and scarcity pose serious challenges for its widespread use in commercial applications. Thus, the need for a low-cost but efficient electrocatalyst for hydrazine oxidation is essential for the further development of hydrazine-based direct liquid fuel cells.[3] In response, various earth-abundant low-cost metallic catalysts have been extensively explored by various research groups around the globe, but these catalysts suffer from poor stability due to the formation of inactive oxide layers on their surfaces during or before the oxidation step of

hydrazine.[4] On the other hand, carbon-based nanomaterials (graphene, carbon nanotubes and mesoporous carbon) present a solution to these issues partially because of their stability in strongly alkaline and acidic conditions.[5] Moreover, these materials possess high intrinsic electrical conductivity that facilitates the electron transfer processes for hydrazine oxidation along with high surface area.[6] These striking properties have led to the use of carbon-based materials for various fuel-cell technologies, including hydrazine fuel cells. For instance, Li *et al.*[7] showed that a complex of graphene and carbon nanotubes can be effectively utilized for the oxygen reduction reaction on the anode side of the fuel cell. Meng *et al.*[4] utilized mesoporous carbon for hydrazine oxidation with an onset potential of only − 0.36 vs saturated calomel electrode (SCE), which is the lowest value achieved for carbon-based materials. However, there is still considerable room for further development of carbon-based electrocatalysts for various fuel-cell applications, including hydrazine oxidation, based on the following aspects. First, apart from the high intrinsic conductivity of carbon-based materials, the utilization of a binder is necessary for most of these nanocatalysts simply because of their powdered nature.[4,5,8] Hence, the added 'dead volume' reduces the number of available active sites for hydrazine oxidation despite the high intrinsic surface area of these nanomaterials often prepared at high temperatures. Second, in particular for hydrazine oxidation, the onset potential is still higher for reported carbon-based materials, which ultimately hampers the overall energy conversion efficiency of these liquid-based fuel cells. Thus, it is imperative to come up with approaches that can

[1]Department of Physics and Graphene Research Institute, Sejong University, Seoul, Korea; [2]School of Materials Science and Engineering, Ulsan National Institute of Science and Technology (UNIST), Ulsan, Korea and [3]Institute of Physics and Applied Physics, Yonsei University, Seoul, Korea
Correspondence: Professor S-H Chun, Department of Physics and Graphene Research Institute, Sejong University, 209 Neungdongro Gwangjingu, Seoul 05006, Korea.
E-mail: schun@sejong.ac.kr

2

shift the onset potential toward a lower and more negative value to achieve better performance for hydrazine-based fuel cells.

Despite tremendous progress in the quest of novel catalysts for hydrazine oxidation, little attention has been devoted to gas management on the surfaces of electrodes.[9] During the oxidation of hydrazine, the released nitrogen gas gradually accumulates on the surface of the electrode and blocks and reduces its catalytically active accessible surface area available for the hydrazine fuel, which ultimately leads to deteriorated performance of the fuel cell. This accumulation/adhesion of gas bubbles is the result of a balance between their 'superaerophobic pinning state' and 'superaerophilic bursting state'.[9,10] Both recent reports and our work suggest that designing an ultra-rough, vertical, nanoarchitecture surface will result in a 'superaerophobic' effect that operates via the creation of a discontinuous three-phase (solid–liquid–gas) contact line (TPCL).[11] For example, Lu et al.[11] showed that three-dimensional nanoporous electrodeposited copper exhibited a superaerophobic effect and superior electrochemical performance for hydrazine oxidation, owing to its highly rough nanostructured surface. Similar results have been shown for vertically aligned MoS_2 toward the hydrogen evolution reaction.[10] All these electrodes possessed discontinuous TPCLs, owing to their ultra-rough surfaces, which then gave birth to superaerophobic properties of the electrodes. Thus, a discontinuous TPCL is imperative for a superaerophobic electrode material, and one of the routes to design such a discontinuous TPCL surface is limiting the growth of a two-dimensional (2D) material in the vertical direction.[10] Graphene, compared to its other carbon counterparts, is unique because of its exceptional electrical properties, huge surface area ($> 2600 \, m^2 \, g^{-1}$) and 2D nature, and thus has been explored extensively for various fuel-cell applications.[12–14] However, for catalytic applications, it has been shown that graphene is highly active at its edges compared to its basal plane.[15,16] The increased density of states at the edge defects compared to basal plane makes the edges of graphene have faster capabilities of electron transfer to oxidize or reduce various chemical compounds in the solution phase. This faster electron transfer ultimately leads to higher current density along with a shift in peak potential. Therefore, conceptually, approaches that can maximize the number of edges on graphene while retaining its high electrical conductivity would ultimately result in high catalytic activity for various fuel-cell applications.[17,18] This, in particular, has led us to explore vertically oriented graphene for its use in hydrazine fuel-cell application because of its maximum number of available active edges for catalysis. Moreover, vertically oriented graphene possesses the ability to address the adhesion of N_2 gas bubbles, owing to its highly rough nano-edge and discontinuous TPCL surface. Hence, the freestanding, vertically oriented graphene electrode can act as a superaerophobic electrode, where gas bubbles quickly leave the surface owing to their exceedingly low contact area with the solid electrode. Moreover, vertical graphene, due to its metal-free nature, is definitely a better choice from a sustainability point of view along with its inherit corrosion stability in strongly alkaline environments where most metals fail to operate, making it an ideal candidate for various fuel-cell technologies.

Herein, we utilized a plasma-enhanced chemical vapor deposition (PECVD) method to directly grow vertically oriented graphene on an insulator (SiO_2/Si) (see Supplementary Figure S1 for schematics and Supplementary Table S1 for growth parameters). The direct growth by PECVD was chosen for its cleaner in situ growth environment, which can eliminate the tedious transfer process of conventional graphene grown on metallic surfaces and hence assures the absence of leftover polymer debris (usually polymethyl methacrylate (PMMA)) on its surface. In addition, the direct growth on an insulator avoids the usage of a sacrificial metal and gives a freestanding electrode with a preserved vertical graphene morphology, which can be directly utilized as an electrode material without the need for additional treatment. The morphology of the resulting graphene resembled closely packed nano-hills with numerous active graphene edges available for hydrazine oxidation. The resulting freestanding vertical graphene electrode exhibited an onset potential of as low as $-0.42 \, V$ (vs SCE) for hydrazine oxidation. To the best of our knowledge, this is the lowest onset potential value reported for hydrazine oxidation for graphene-based electrode materials. In addition, the obtained current densities were also superior among the reported carbon-based electrocatalysts for hydrazine oxidation. Furthermore, for the first time, we show that the vertical graphene electrode can act as a 'superaerophobic electrode', and thus can accelerate the process of the removal of N_2 gas bubbles produced on its surface when utilized as an anode in a hydrazine fuel cell.

MATERIALS AND METHODS

Experimental section

An SiO_2 (300 nm)/n-Si wafer purchased from Dasom RMS (Seoul, Korea) was used as a substrate for the growth of graphene by the PECVD method. Prior to graphene growth, O_2 gas was introduced into the chamber at a low rate of 50 standard cubic centimeters per min (s.c.c.m.) and discharged at an radio frequency (RF) power of 50 W for 3 min to remove any organic materials contaminating the surface. The growth of flat graphene was achieved by our previously established method.[19,20] Briefly, the substrate temperature was maintained at 500 °C for 3 h, and an RF plasma was generated within the chamber by the continuous flow of hydrogen (H_2, 20 s.c.c.m.) and methane (CH_4, 2 s.c.c.m.), while maintaining the chamber pressure at 10 mTorr. The resolutions of the mass flow controllers were 1 s.c.c.m. for hydrogen and 0.1 s.c.c.m. for methane. Subsequently, the sample was cooled rapidly to room temperature at a cooling rate of 3 °C s^{-1}. The growth of the vertical graphene nano-hills (VGNH-45) was achieved at relatively higher temperatures (750 °C) than flat graphene but for a shorter period of time (45 min). The flow of methane was increased to 10 s.c.c.m., whereas the hydrogen flow was maintained at the previous value of 20 s.c.c.m. The rest of the procedure remained the same. VGNH-60 was also grown for comparison purposes with a longer period of time (see details in Supplementary Table S1).

Materials characterizations

Scanning electron microscopy was performed with a JEOL JSM-7001F (JEOL, Tokyo, Japan) at an acceleration voltage of 10 kV. For high-resolution transmission electron microscopy (TEM) measurements, VGNH-45 grown on the SiO_2/Si substrate was transferred onto a TEM grid by a wet direct-transfer method for TEM analysis. The wet direct-transfer method without polymer coating was adopted for reducing polymer residue. Isopropyl alcohol was dropped on the top of the grid to bond between the sample and the TEM grid. Then, a KOH solution was used for detaching the TEM grid bonded with the sample by etching the SiO_2 substrate. Finally, distilled water was used for rinsing the KOH residue from the sample. High-resolution TEM images were obtained on an FEI Titan G2 60-300 (FEI, Hillsboro, OR, USA) operated at an 80-kV acceleration voltage to decrease beam damage to the samples. The surface morphology of the samples was evaluated using a commercial atomic force microscopy (PSIA, Park Systems, Suwon, Korea, XEI100). X-ray photoelectron spectroscopy was performed using a K-alpha (Thermo VG, East Grinstead, UK) X-ray photoelectron spectrometer with a monochromatic Al X-ray source with 12-kV power. Raman spectroscopy (Renishaw, Gloucestershire, UK) with an excitation wavelength of 514.5 nm was used to confirm the growth and stability of graphene. The nitrogen bubble-releasing images were recorded using a high-speed charge-coupled device camera mounted on a microscope (Olympus, Tokyo, Japan, BX-51).
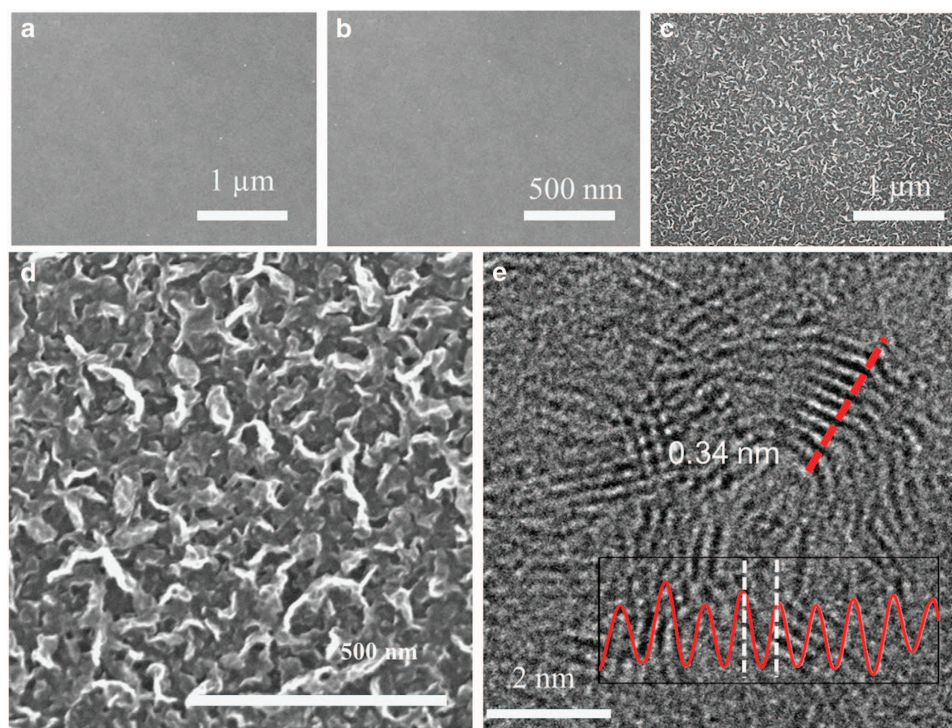
Figure 1 Field-emission scanning electron microscopic images of (**a**, **b**) the direct growth of flat graphene on SiO$_2$/Si, showing an ultra-smooth, flat surface and (**c**, **d**) the direct growth of vertical graphene nano-hills at 750 °C on SiO$_2$/Si for 45 min, showing the vertical nature of graphene. (**e**) HR-TEM images of VGNH-45, showing the average number of graphene layers present on the edge.

Electrochemical characterizations

All electrochemical measurements were carried out with a Biologic SP-300 workstation (Bio-Logic Science Instruments, Seyssinet-Pariset, France). The working electrode was either Si/SiO$_2$/planar graphene or Si/SiO$_2$/vertical graphene and was directly used without additional treatment. Cyclic voltammograms were recorded in 0.1 M KOH solution containing 50 mM hydrazine monohydrate using a SCE as the reference electrode and a graphite rod as the counter electrode.

RESULTS

The direct growth of VGNHs on an insulator substrate was optimized at a relatively lower temperature of 750 °C for 45 min (herein referred as VGNH-45) compared to its growth on metallic surfaces (normally 1000 °C), which is an added advantage of the utilization of the PECVD method. For comparison purposes, flat/planar few-layer graphene (FG) was grown on SiO$_2$/Si by our previously reported method.[19] Growth was performed using methane as a carbon precursor along with hydrogen at a plasma power of 50 W (see Materials and methods for details). VGNHs were also grown for a longer growth time of 1 h (VGNGs-60) to assess the growth parameters for the VGNHs and their further utilization for hydrazine oxidation.

The field-emission scanning electron microscopic images of FG and VGNH-45 are shown in Figure 1. It is evident that FG (Figures 1a and b) shows a clear and smooth surface even at higher magnifications, confirming its flat nature, whereas VGNH-45 exhibits (Figures 1c and d) an extremely rough surface with clearly visible vertical nanosheets covering the entire surface of the insulator.[21] Supplementary Figure S2 further compares VGNH-45 with VGNH-60. For a longer growth time of 60 min, less dense and wide clusters of the VGNHs are observed for VGNH-60. Furthermore, high-resolution TEM analysis of VGHNs-45 (Figure 1e; Supplementary

Figure S3) shows that the number of graphene layers on the edges are between six and nine layers. We also confirm that the spacing between each layer (0.34 nm) corresponds to the typical spacing of multilayer graphene. Supplementary Figure S4 shows typical Raman spectra of VGNH-45 and FG grown by PECVD.[20,22] The G and 2D bands appear at ~ 1580 and 2700 cm^{-1}, respectively, whereas the D band is located at ~ 1350 cm^{-1}. The presence of a clear 2D peak confirms the formation of graphene sheets in both samples.[21] The FG was identified in our previous study to have three to four graphene layers formed on metal-catalyst-free substrates in a planar manner with structural disorders.[20] The decreased I_{2D}/I_G ratio (0.28) in VGNH-45 suggests its multilayer nature and a reduced lateral coherence length because of vertical termination.[23,24,25] The large I_D/I_G ratio in both samples indicates the presence of defects within the graphene sheets, which are indeed beneficial for electrocatalytic reactions.

To further evaluate the morphology of the VGNHs, atomic force microscopy was utilized, as shown in Figure 2. The flat graphene exhibits an ultra-smooth surface with an average height of 2 nm, suggesting interconnected graphene sheets oriented horizontally to the SiO$_2$ surface. In contrast, the surface of VGNH-45 exhibits high roughness with vertically oriented graphene nano-hills as high as 31 nm with an average height of 15 nm. The corresponding three-dimensional atomic force microscopy image of VGNH-45 clearly shows the nano-hill morphology of the vertical graphene with numerous nanometer-sized connected valleys and peaks, creating a continuous nanosized mountainous region. Apart from the difference in morphology between FG and VGNH-45, their chemical nature remains the same, as evidenced from the X-ray photoelectron spectroscopy spectra of C 1s shown in Supplementary Figure S6.[26,27] The tail between 286 and 290 eV refers to C−O, C=O, and energy-loss 'shake-up' features.[22] Furthermore, the X-ray photoelectron
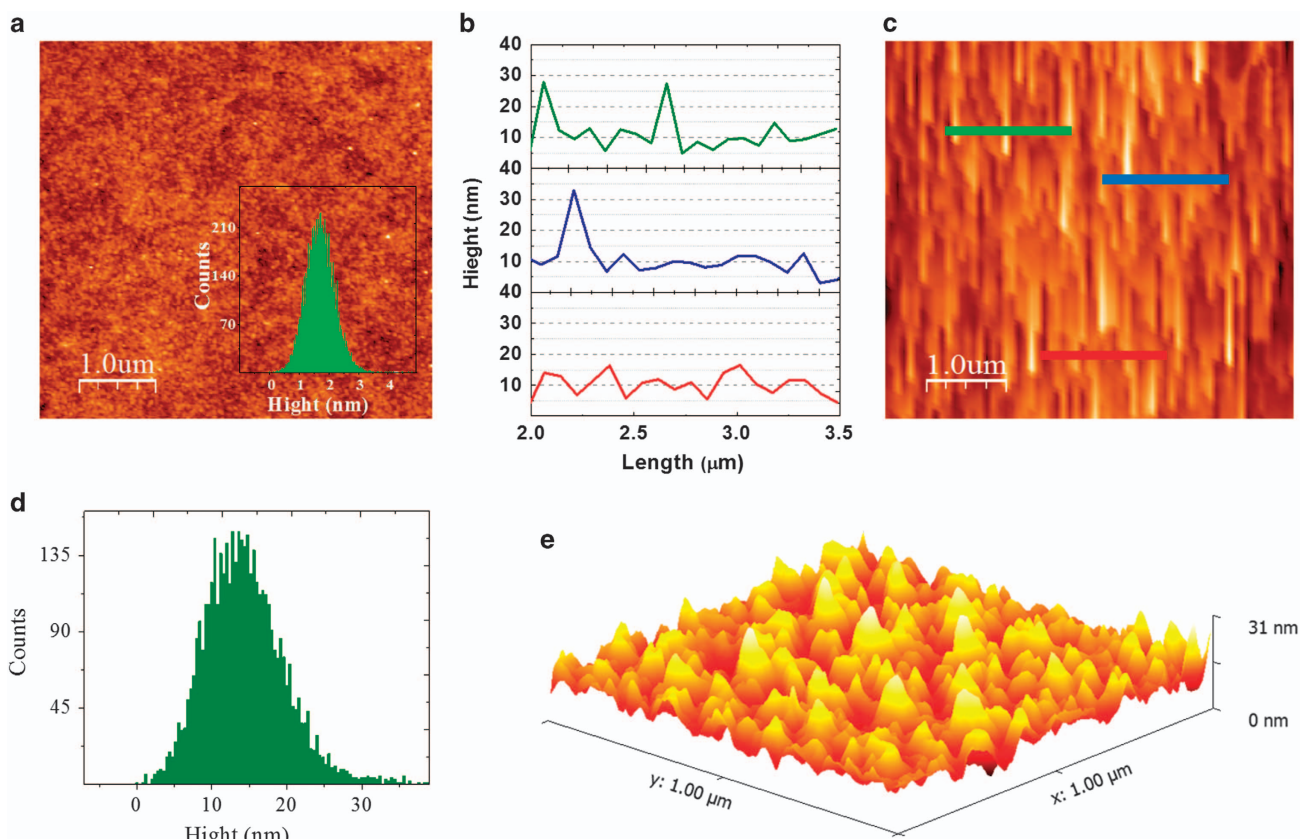
Figure 2 (**a**) Atomic force microscopy (AFM) image of FG on SiO₂/Si with an inset showing the height histogram. (**b**, **c**) AFM image of VGNH-45 grown on an insulator substrate and their corresponding line profiles at different locations, showing that the height of graphene nano-hills ranges between 10 and 20 nm with some peaks going beyond 30 nm in height. (**d**) Height histogram obtained from (**b**, **e**) the corresponding 3D AFM image of (**b**), showing the nano-hill morphology of VGNH-45.

spectroscopy survey spectrum of VGNH-45 (Supplementary Figure S7) shows a strong C 1s peak at 285 eV, a Si 2p3 peak at 102 eV due to the SiO₂/Si substrate, a small O 1s peak at 533 eV and a weak O KLL Auger band between 970 and 980 eV. The presence of O 1s is due to oxygen adsorbates on the film surface when the sample is exposed to ambient conditions and oxygen in the substrate.[22] Quantitatively, a maximum percentage of 95.03% was found for carbon, whereas only 3.36% was assigned to oxygen, and the rest was assigned to Si.

Further comparison of VGNH-45 with VGNH-60 (Supplementary Figure S5) reveals that the former possesses sharper and denser nano-hills, hence providing a greater number of catalytically active sites for hydrazine oxidation while maintaining its interconnected network of graphene sheets beneath the critical height of 15 nm, which is the approximate height of interconnected graphene valleys. This network is essential for the better interconnectivity of individual graphene hills so that they remain electrically connected one another and to the external connection. Both VGNH-45 and VGNH-60 possess this critical height area, but the peaks of VGNH-60 are much broader than those of VGNH-45 due to the longer growth time. These atomic force microscopy images corroborate with the field-emission scanning electron microscopic data (Supplementary Figure S2) and show that, as the growth time increases, the peaks become broader with longer edges, which ultimately results in the reduction of the total surface area.

The catalytic activity of hydrazine oxidation was further assessed by cyclic voltammetry, as shown in Figure 3a and Supplementary

Figure S8. The onset potential for hydrazine oxidation of VGNH-45 was − 0.42 V (vs SCE), which is much lower than − 0.21 V (vs SCE) observed for FG. Moreover, the increase in current density of VGNH-45 is much sharper than FG, suggesting that graphene possesses a higher catalytic activity on its edges compared to its basal plane. It is worth mentioning here that a higher current density (13 mA cm⁻² vs SCE at 0 V with a scan rate of 50 mV s⁻¹) and a lower onset potential (−0.42 V vs SCE) were observed for our VGNH-45 compared to various carbon-based materials utilized for hydrazine oxidation, making it one of the best reported carbon-based materials for hydrazine oxidation. For instance, poorer current density (~5 mA cm⁻² vs SCE at 0 V with a scan rate of 50 mV s⁻¹) and higher onset potential (−0.36 V vs SCE) were observed for the dual-doped mesoporous carbon reported by Meng et al.[4] compared to our VGNH-45 freestanding electrode. Furthermore, our electrode takes advantage of its facile direct growth avoiding the utilization of binding agents that lead to deteriorated performance toward hydrazine oxidation. Similarly, VGNH-45 outperforms the fibrous porous carbon electrocatalysts reported by Martins et al.[28] both in current density (~4 mA cm⁻² vs SCE at 0.1 V with a scan rate of 50 mV s⁻¹) and onset potential (−0.3 V vs SCE). Furthermore, VGNH-45 exhibits the lowest onset potential among previously published metallic/non-metallic electrocatalysts for hydrazine oxidation (Supplementary Table S2), making it one of the best available electrocatalysts for hydrazine oxidation.

Figure 3b and Supplementary Figure S9 further compare the observed current densities obtained from the cyclic voltammograms
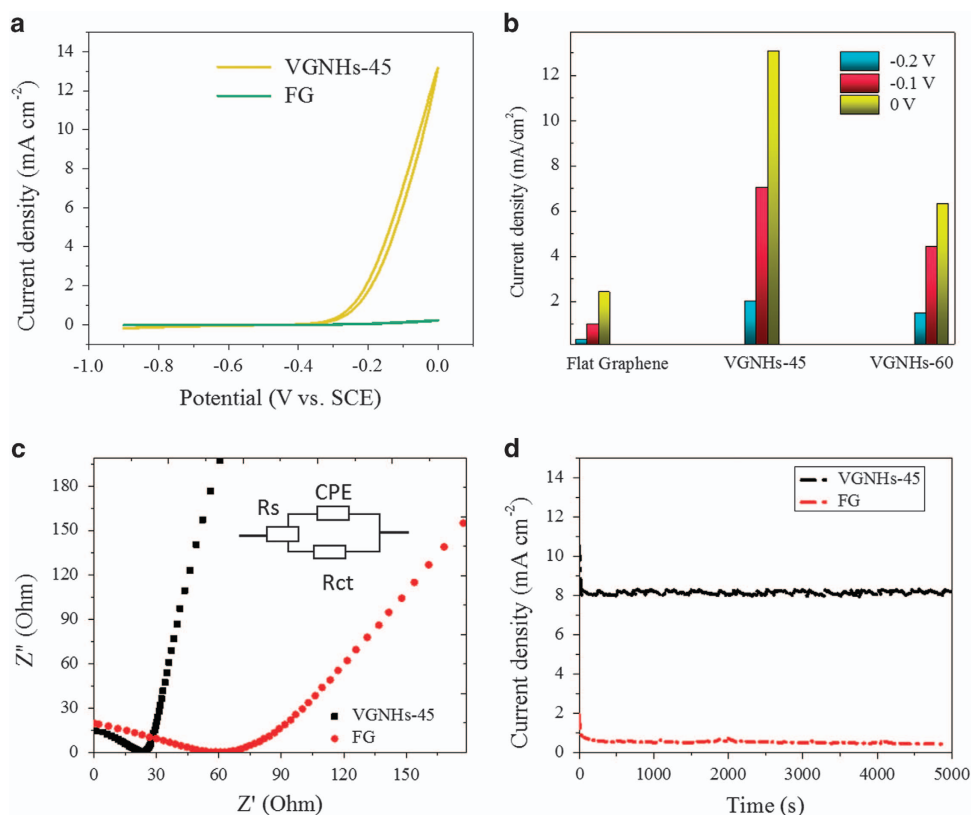
Figure 3 (**a**) Cyclic voltammograms of VGNH-45 and FG in 0.1 M KOH containing 50 mM hydrazine monohydrate solution, showing the higher current density and the lower onset potential for hydrazine oxidation for VGNH-45. (**b**) Comparison of the current densities at various voltages for FG, VGNH-45 and VGNH-60 obtained from the corresponding cyclic voltammograms, showing the better performance of VGNH-45 compared to the others. (**c**) Comparison of the impedances of VGNH-45 and FG in 0.1 M KOH containing 50 mM hydrazine at the open-circuit potential. (**d**) Chronoamperograms of VGNH-45 and FG, showing the long-term cyclic stability for hydrazine oxidation. The higher current density for VGNH-45 at 0 V vs SCE shows its better performance and stability for hydrazine oxidation.

of the different electrodes. It is evident that VGNH-45 shows markedly improved current density at various voltages compared to VGNH-60. This reduction in catalytic activity of VGNH-60 is expected due to the larger grains of the vertical graphene owing to its longer growth time (Supplementary Figures S2 and S5). These larger VGNHs have reduced surface area owing to their broader shape and hence provide a smaller number of catalytically active sites for hydrazine oxidation compared to VGNH-45, which contains shaper nano-hill edges.

Electrochemical impedance spectroscopy was further employed to study the electrode kinetics of hydrazine oxidation of our electrode materials. Nyquist plots (Figure 3c) of similar shape were observed for both FG and VGNH-45, suggesting similar electrode kinetics in both samples.[29] However, the smaller semicircle of VGNH-45 compared to FG indicates a much lower value of charge-transfer resistance (Rct from the equivalent circuit) and hence faster kinetics, which ultimately results in its greater performance toward hydrazine oxidation compared to flat graphene.[29]

The stabilities of VGNH-45 and FG were tested by chronoamperometry, as shown in Figure 3d and Supplementary Figure S10. It is evident that both FG and VGNH-45 are able to retain > 80% of their initial current densities, indicating that their stability is suitable for hydrazine oxidation. The higher current density observed for VGNH-45 again proves its better performance against FG. Comparison of the Raman spectra of VGNH-45 before and after the chronoamperometric studies (Supplementary Figure S11) also suggests that the VGNH-45 electrode is stable in prolonged hydrazine

oxidation conditions. Similar levels of stability have been found from vertical structures of 2D materials, including graphene.[30,31] Moreover, the diffusion constant for VGNH-45 was calculated based on the Cottrell equation (see Supplementary Information for details) and was found to be 4.04×10^{-10} cm^2 s^{-1}, which is much lower compared to previous values, making it a promising electrocatalyst for hydrazine oxidation.[4,5] Furthermore, the activation energy values of FG and VGNH-45 for oxidation were estimated according to the previously reported Arrhenius equation.[32] A small activation energy of 18.07 kJ mol^{-1} was observed for VGNH-45 compared to the much larger value of 39.28 kJ mol^{-1} for FG electrode (Supplementary Figures S12 and S13). These findings indeed support that the VGNH-45 electrode has faster kinetics for hydrazine oxidation compared to FG. In addition, the value is even comparable to those of other metallic electrodes used for hydrazine oxidation, indicating that our VGNH-45 possesses superior advantages owing to its metal-free nature.[32,33]

For a quantitative comparison of the 'superaerophobic' effect of FG vs VGNH-45, a digital recording process was adopted, and the results are displayed in Figure 4. For FG (Figures 4d–f), the N$_2$ gas bubbles grow larger in size (before they leave the surface of electrode) with an average diameter of ~ 300 µm, whereas for VGNH-45 (Figures 4a–c), the bubble size remains confined to an average diameter of ~ 40 µm. Moreover, in a certain given area, numerous smaller bubbles were found on the surface of VGNH-45 compared to only one larger bubble on FG (Supplementary Video 1). The presence
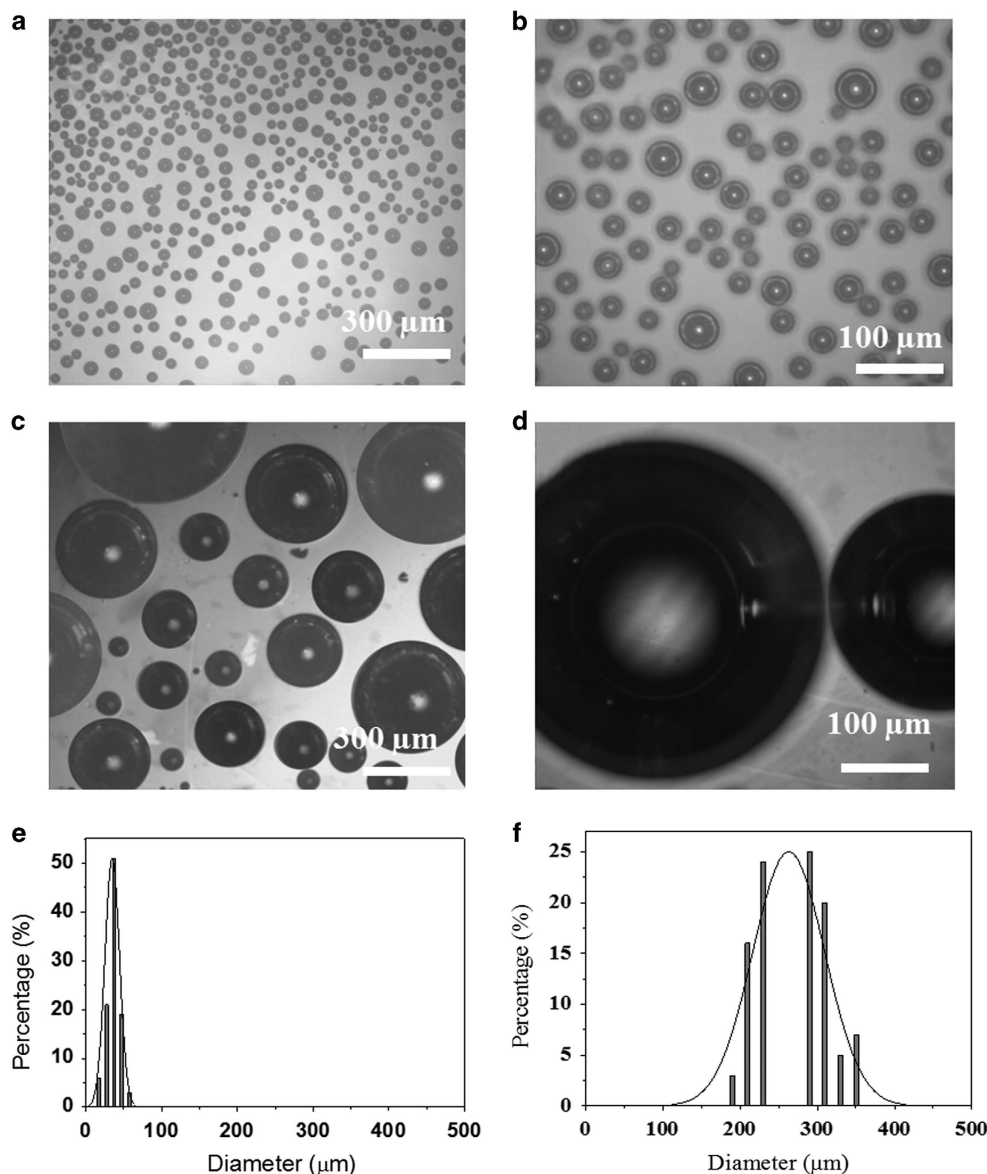
Figure 4 Digital images showing the size of N$_2$ bubbles produced on the electrode surface during hydrazine oxidation for (**a**, **b**) VGNH-45 and (**c**, **d**) FG. The corresponding statistical distributions of the bubble size are presented at the right for (**e**) VGNH-45 and (**f**) FG. These data clearly show that the bubble size released from VGNH-45 is approximately eight times smaller in diameter compared to those produced from the flat graphene electrode surface, which ultimately gives it 'superaerophobic' properties and hence results in its higher performance toward hydrazine oxidation.

of numerous densely packed smaller bubbles on the surface of VGNH-45 indicates the availability of a larger number of catalytically active site for hydrazine oxidation compared to FG. The smaller size of the gas bubbles for VGNH-45 is the result of broken TPCL on the surface of the electrode (Figure 5b) compared to the continuous TPCL in the flat graphene electrode (Figure 5a).[9,10,29] This broken TPCL results in a smaller adhesion force of gas bubbles on the surface of the electrode, which eventually leads them to leave the surface quickly (Supplementary Video 2), hence improving the current density of the electrode toward hydrazine oxidation. The broken TPCL arises due to the highly rough nanoscale morphology of the vertically oriented graphene nano-hills. Thus, the nano-hill morphology of graphene proves to be essential for efficient gas evolution by preventing the adhesion of bubbles on the electrode surface and hence improving

the overall efficiency toward hydrazine oxidation. Furthermore, the comparison of the bubble sizes between VGNH-45 and VGNH-60 (Supplementary Figure S14) shows that comparatively larger-sized bubbles appear on VGNH-60. This is due to the larger and broader peaks of VGNH-60 (Supplementary Figures S2 and S5), which results in an increase of the bubble size on its surface compared to VGHN-45. Furthermore, Supplementary Figure S15 shows that the onset potential shifts toward a more positive value as the bubble size increases. This suggests a possible correlation between the onset potential and the bubble size (or superaerophobicity), and hence provides a new route to minimize the onset potential for various electrocatalytic reactions that produce bubbles. Thus, former studies and our work indicate that superaerophobicity is an important factor in attaining low onset potentials.[10]
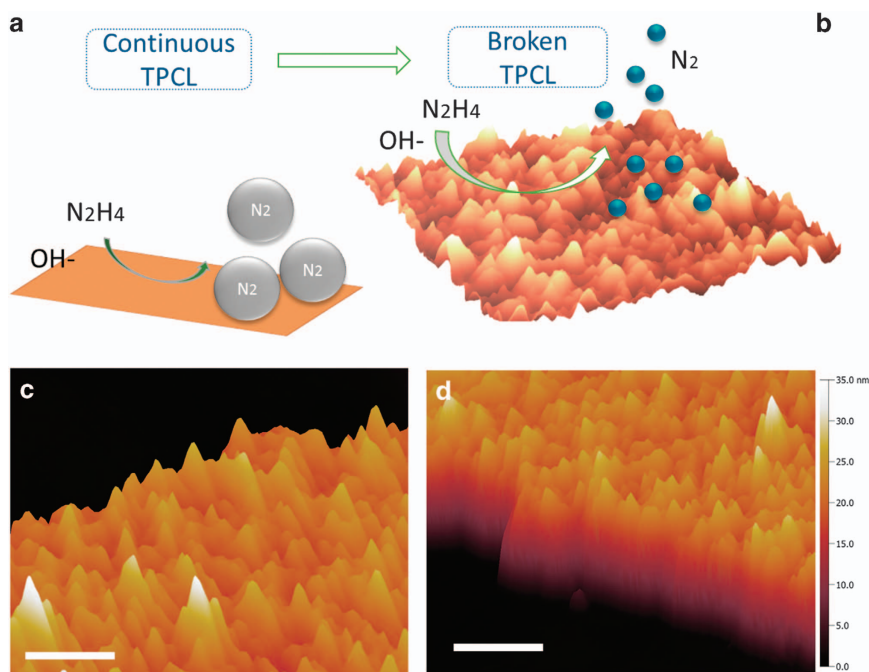
Figure 5 Mechanistic illustration of hydrazine oxidation on (**a**) FG with continuous TPCL and (**b**) VGNH-45 with broken TPCL due to its nano-rough surface. (**c**, **d**) Magnified 3D AFM micrographs of VGNH-45 from different perspectives, showing densely packed, continuous nano-hills with numerous vertical edges available for hydrazine oxidation. The scale bar is 300 nm in both images.

DISCUSSION

The sharp increase in current density and the low onset potential compared to that observed in other studies might be the result of a combination of various factors, such as (1) the presence of a vast number of catalytically active sites available for hydrazine oxidation on VGNH-45 due to its nano-edged vertical structure compared to FG, which cannot offer a large number of catalytically active sites owing to its planar orientation; (2) the presence of a dense network of interconnected graphene nanosheets underneath the nano-peaks (15-nm critical height), providing ultra-fast base conductivity, which then facilitates the faster transfer of electrons to and from the peaks to the base of the electrode for efficient hydrazine oxidation; and (3) the direct growth of 3D vertical graphene on the insulator and its direct use as a freestanding electrode for hydrazine oxidation, which allows it to maintain its structural integrity with nanoporosity and maximize the available active surface area for the oxidation of hydrazine. Our direct growth of vertical graphene by PECVD is in contrast to the traditional powdered carbon-based materials, which ultimately need to be fixated on conductive substrates prior to their utilization as electrodes. These methods result in a loss of structural integrity along with a loss of sufficient available active surface area. Moreover, further mixing of binding agents increases the inactive volume and results in poor catalytic activity, as evidenced in other studies.[4,8,28]

The inherent superaerophobic characteristics of our vertical graphene further facilitate and enhance the electro-oxidation of hydrazine on the electrode surface by swiftly removing the nitrogen bubbles produced on its surface. Such swift removal is the result of the creation of a discontinuous TPCL layer on the electrode surface, which then effectively shifts the potential toward a more negative onset value during electro-oxidation. These characteristics arise due to the nano-hill morphology of the vertical graphene having an ultra-rough nano-edged surface. This superaerophobicity also helps the physical stability over prolonged time because smaller bubbles are adsorbed on the surface with smaller adhesion energies, which reduces the possibility of detachment of the vertically standing graphene.

In conclusion, the growth of VGNHs was achieved by PECVD method on an insulator surface. The resulting substrate was then utilized as a freestanding electrode for hydrazine oxidation. This metal-free vertical graphene electrocatalyst outperformed the previously reported carbon-based electrocatalysts in terms of both onset potential and current density. In addition, for the first time, it was shown that the VGNHs act as a superaerophobic electrode by the creation of a discontinuous TPCL layer on its surface during hydrazine oxidation. Such a discontinuous TPCL layer quickly removes N_2 bubbles produced on the electrode surface, which results in higher electrode efficiencies. We believe that our current findings will inspire the utilization of nano-rough surfaces for other electrocatalytic applications.

CONFLICT OF INTEREST

The authors declare no conflict of interest.

1 Yu, E. H., Wang, X., Krewer, U., Li, L. & Scott, K. Direct oxidation alkaline fuel cells: from materials to systems. *Energy Environ. Sci.* **5**, 5668 (2012).

2 Serov, A., Padilla, M., Roy, A. J., Atanassov, P., Sakamoto, T., Asazawa, K. & Tanaka, H. Anode Catalysts for Direct Hydrazine Fuel Cells: From Laboratory Test to an Electric Vehicle. *Angew. Chem. Int. Ed.* **53**, 10336–10339 (2014).

3 Serov, A. & Kwak, C. Direct hydrazine fuel cells: a review. *Appl. Catal. B Environ.* **98**, 1–9 (2010).

4 Meng, Y., Zou, X., Huang, X., Goswami, A., Liu, Z. & Asefa, T. Polypyrrole-derived nitrogen and oxygen co-doped mesoporous carbons as efficient metal-free electrocatalyst for hydrazine oxidation. *Adv. Mater.* **26**, 6510–6516 (2014).

5 Yu, D., Wei, L., Jiang, W., Wang, H., Sun, B., Zhang, Q., Goh, K., Si, R. & Chen, Y. Nitrogen doped holey graphene as an efficient metal-free multifunctional electrochemical catalyst for hydrazine oxidation and oxygen reduction. *Nanoscale* **5**, 3457–3464 (2013).

6 Kim, K., Lee, T., Kwon, Y., Seo, Y., Song, J., Park, J. K., Lee, H., Park, J. Y., Ihee, H., Cho, S. J. & Ryoo, R. Lanthanum-catalysed synthesis of microporous 3D graphene-like carbons in a zeolite template. *Nature* **535**, 131–135 (2016).

7 Li, Y., Zhou, W., Wang, H., Xie, L., Liang, Y., Wei, F., Idrobo, J.-C., Pennycook, S. J. & Dai, H. An oxygen reduction electrocatalyst based on carbon nanotube–graphene complexes. *Nat. Nanotechnol.* **7**, 394–400 (2012).

8 Wang, Y., Wan, Y. & Zhang, D. Reduced graphene sheets modified glassy carbon electrode for electrocatalytic oxidation of hydrazine in alkaline media. *Electrochem. Commun.* **12**, 187–190 (2010).

9 Li, Y., Zhang, H., Xu, T., Lu, Z., Wu, X., Wan, P., Sun, X. & Jiang, L. Under-water superaerophobic pine-shaped pt nanoarray electrode for ultrahigh-performance hydrogen evolution. *Adv. Funct. Mater.* **25**, 1737–1744 (2015).

10 Lu, Z., Zhu, W., Yu, X., Zhang, H., Li, Y., Sun, X., Wang, X., Wang, H., Wang, J., Luo, J., Lei, X. & Jiang, L. Ultrahigh hydrogen evolution performance of under-water 'superaerophobic' MoS₂ nanostructured electrodes. *Adv. Mater.* **26**, 2683–2687 (2014).

11 Lu, Z., Sun, M., Xu, T., Li, Y., Xu, W., Chang, Z., Ding, Y., Sun, X. & Jiang, L. Superaerophobic electrodes for direct hydrazine fuel cells. *Adv. Mater.* **27**, 2361–2366 (2015).

12 Yeh, T.-F., Teng, C.-Y., Chen, S.-J. & Teng, H. Nitrogen-doped graphene oxide quantum dots as photocatalysts for overall water-splitting under visible light illumination. *Adv. Mater.* **26**, 3297–3303 (2014).

13 Fei, H., Dong, J., Arellano-Jiménez, M. J., Ye, G., Dong Kim, N., Samuel, E. L. G., Peng, Z., Zhu, Z., Qin, F., Bao, J., Yacaman, M. J., Ajayan, P. M., Chen, D. & Tour, J. M. Atomic cobalt on nitrogen-doped graphene for hydrogen generation. *Nat. Commun.* **6**, 8668 (2015).

14 Zhang, J., Zhao, Z., Xia, Z. & Dai, L. A metal-free bifunctional electrocatalyst for oxygen reduction and oxygen evolution reactions. *Nat. Nanotechnol.* **10**, 444–452 (2015).

15 Yuan, W., Zhou, Y., Li, Y., Li, C., Peng, H., Zhang, J., Liu, Z., Dai, L. & Shi, G. The edge- and basal-plane-specific electrochemistry of a single-layer graphene sheet. *Sci. Rep.* **3**, 1–7 (2013).

16 Li, W., Tan, C., Lowe, M. a., Abruña, H. D. & Ralph, D. C. Electrochemistry of individual monolayer graphene sheets. *ACS Nano* **5**, 2264–2270 (2011).

17 Wang, H., Kong, D., Johanes, P., Cha, J. J., Zheng, G., Yan, K., Liu, N. & Cui, Y. MoSe₂ and WSe₂ nanofilms with vertically aligned molecular layers on curved and rough surfaces. *Nano Lett.* **13**, 3426–3433 (2013).

18 Xia, J., Chen, F., Li, J. & Tao, N. Measurement of the quantum capacitance of graphene. *Nat. Nanotechnol.* **4**, 505–509 (2009).

19 Kim, Y. S., Joo, K., Jerng, S. K., Lee, J. H., Moon, D., Kim, J., Yoon, E. & Chun, S. H. Direct integration of polycrystalline graphene into light emitting diodes by plasma-assisted metal-catalyst-free synthesis. *ACS Nano* **8**, 2230–2236 (2014).

20 Kim, Y. S., Joo, K., Jerng, S.-K., Lee, J. H., Yoon, E. & Chun, S.-H. Direct growth of patterned graphene on SiO₂ substrates without the use of catalysts or lithography. *Nanoscale* **6**, 10100 (2014).

21 Li, M., Liu, D., Wei, D., Song, X., Wei, D. & Wee, A. T. S. Controllable synthesis of graphene by plasma-enhanced chemical vapor deposition and its related applications. *Adv. Sci.* **3**, 1600003 (2014).

22 Jiang, L., Yang, T., Liu, F., Dong, J., Yao, Z., Shen, C., Deng, S., Xu, N., Liu, Y. & Gao, H. J. Controlled synthesis of large-scale, uniform, vertically standing graphene for high-performance field emitters. *Adv. Mater.* **25**, 250–255 (2013).

23 Das, A., Chakraborty, B. & Sood, A. K. Raman spectroscopy of graphene on different substrates and influence of defects. *Bull. Mater. Sci.* **31**, 579–584 (2008).

24 Jacob, M. V., Rawat, R. S., Ouyang, B., Bazaka, K., Kumar, D. S., Taguchi, D., Iwamoto, M., Neupane, R. & Varghese, O. K. Catalyst-free plasma enhanced growth of graphene from sustainable sources. *Nano Lett.* **15**, 5702–5708 (2015).

25 Ghosh, S., Ganesan, K., Polaki, S. R., Ravindran, T. R., Krishna, N. G., Kamruddin, M. & Tyagi, A. K. Evolution and defect analysis of vertical graphene nanosheets. *J. Raman Spectrosc.* **45**, 642–649 (2014).

26 Jin, Z., Yao, J., Kittrell, C. & Tour, J. M. Large-scale growth and characterizations of nitrogen-doped monolayer graphene sheets. *ACS Nano* **5**, 4112–4117 (2011).

27 Ito, Y., Christodoulou, C., Nardi, M. V., Koch, N., Sachdev, H. & Müllen, K. Chemical vapor deposition of n-doped graphene and carbon films: the role of precursors and gasphase. *ACS Nano* **8**, 3337–3346 (2014).

28 Martins, A. C., Huang, X., Goswami, A., Koh, K., Meng, Y., Almeida, V. C. & Asefa, T. Fibrous porous carbon electrocatalysts for hydrazine oxidation by using cellulose filter paper as precursor and self-template. *Carbon* **102**, 97–105 (2016).

29 Lu, Z., Sun, M., Xu, T., Li, Y., Xu, W., Chang, Z., Ding, Y., Sun, X. & Jiang, L. Superaerophobic electrodes for direct hydrazine fuel cells. *Adv. Mater.* **27**, 2361–2366 (2015).

30 Kong, D., Wang, H., Cha, J. J., Pasta, M., Koski, K. J., Yao, J. & Cui, Y. Synthesis of MoS2 and MoSe2 films with vertically aligned layers. *Nano Lett.* **13**, 1341–1347 (2013).

31 Mao, S., Wen, Z., Ci, S., Guo, X., Ostrikov, K. K. & Chen, J. Perpendicularly oriented MoSe2 /graphene nanosheets as advanced electrocatalysts for hydrogen evolution. *Small* **11**, 414–419 (2015).

32 Hosseini, M., Momeni, M. M. & Faraji, M. Electro-oxidation of hydrazine on gold nanoparticles supported on TiO 2 nanotube matrix as a new high active electrode. *J. Mol. Catal. A Chem.* **335**, 199–204 (2011).

33 Liu, R., Ye, K., Gao, Y., Zhang, W., Wang, G. & Cao, D. Ag supported on carbon fiber cloth as the catalyst for hydrazine oxidation in alkaline medium. *Electrochim. Acta* **186**, 239–244 (2015).